energies

MDPI

Article

Hydraulic Characterization of the Full Scale Mock-Up of the DEMO Divertor Outer Vertical Target

Amelia Tincani [1], Francesca Maria Castrovinci [2], Moreno Cuzzani [1], Pietro Alessandro Di Maio [2], Ivan Di Piazza [1], Daniele Martelli [1], Giuseppe Mazzone [3], Andrea Quartararo [2] and Eugenio Vallone [2,*] and Jeong-Ha You [4]

1 ENEA FSN-ING CR Brasimone, Camugnano, 40032 Bologna, Italy; amelia.tincani@enea.it (A.T.); moreno.cuzzani@enea.it (M.C.); ivan.dipiazza@enea.it (I.D.P.); daniele.martelli@enea.it (D.M.)
2 Department of Engineering, University of Palermo, Viale delle Scienze, Ed. 6, 90128 Palermo, Italy; francescamaria.castrovinci@unipa.it (F.M.C.); pietroalessandro.dimaio@unipa.it (P.A.D.M.); andrea.quartararo@unipa.it (A.Q.)
3 Department of Fusion and Technology for Nuclear Safety and Security, ENEA C. R. Frascati, Via E. Fermi 45, Frascati, 00044 Roma, Italy; giuseppe.mazzone@enea.it
4 Max Planck Institute of Plasma Physics (E2M), Boltzmann Str. 2, 85748 Garching, Germany; you@ipp.mpg.de
* Correspondence: eugenio.vallone@unipa.it

Abstract: In the frame of the pre-conceptual design activities of the DEMO work package DIV-1 "Divertor Cassette Design and Integration" of the EUROfusion program, a mock-up of the divertor outer vertical target (OVT) was built, mainly in order to: (i) demonstrate the technical feasibility of manufacturing procedures; (ii) verify the hydraulic design and its capability to ensure a uniform and proper cooling for the plasma facing units (PFUs) with an acceptable pressure drop; and (iii) experimentally validate the computational fluid-dynamic (CFD) model developed by the University of Palermo. In this context, a research campaign was jointly carried out by the University of Palermo and ENEA to experimentally and theoretically assess the hydraulic performances of the OVT mock-up, paying particular attention to the coolant distribution among the PFUs and the total pressure drop across the inlet and outlet sections of the mock-up. The paper presents the results of the steady-state hydraulic experimental test campaign performed at ENEA Brasimone Research Center as well as the relevant numerical analyses performed at the Department of Engineering at the University of Palermo. The test facility, the experimental apparatus, the test matrix and the experimental results, as well as the theoretical model, its assumptions, and the analyses outcomes are herewith reported and critically discussed.

Keywords: DEMO; divertor; plasma facing components; thermal hydraulics

Citation: Tincani, A.; Castrovinci, F.M.; Cuzzani, M.; Di Maio, P.A.; Di Piazza, I.; Martelli, D.; Mazzone, G.; Quartararo, A.; Vallone, E.; You, J.-H. Hydraulic Characterization of the Full Scale Mock-Up of the DEMO Divertor Outer Vertical Target. *Energies* **2021**, *14*, 8086. https://doi.org/10.3390/en14238086

Academic Editor: Hyungdae Kim

Received: 29 October 2021
Accepted: 29 November 2021
Published: 2 December 2021

1. Introduction

The pursuit of fusion power is propelled by a call for sustainable and foreseeable low-carbon sources of energy due to the increasing global electricity needs. In this context, Europe has conceived a roadmap [1] that ensures a clear and organized path for proof of commercial electric power production from nuclear fusion facilities, at a reasonable timescale [2]. As an essential element of the European roadmap to the realization of fusion electricity, Europe is leading the design of a DEMO plant, which will be the final pivotal step towards harnessing fusion power after ITER [1].

The DEMO plant is expected to run in the middle of the century, with the main objectives of demonstrating the production of few hundred MWs of net electrical energy, operating with a closed-tritium fuel cycle and maintenance systems capable of achieving acceptable plant availability [3]. The DEMO design and R&D activities in Europe will surely profit from the experiences gained from the design, construction, and operation of ITER. Nevertheless, there are still physics, materials, and engineering challenges that need to be addressed [3].

Among them, the European roadmap to the realization of fusion electricity has defined reliable power exhausting as one of the most decisive missions. The power necessary to maintain plasma at high temperatures has to be exhausted. Heat-exhaust systems have to endure the large heat and particle fluxes of a fusion power plant while ensuring the highest possible performance from the core plasma [1]. The divertor is the fundamental in-vessel component in accomplishing this mission. Being devoted to power exhaust and impurity removal via guided plasma exhaust, the feasibility of fusion power generation depends, to a large extent, on the heat load that can be tolerated by the divertor under normal and off-normal conditions [3].

According to its latest concept, the DEMO divertor is articulated in 48 toroidal assemblies. Each assembly is composed of a cassette body, endowed with a shielding liner, two reflector plates, and two plasma facing components (PFCs), namely an inner vertical target (IVT) and an outer vertical target (OVT) [4]. In the IVT and OVT, there are the plasma facing units (PFUs). These crucial components, adopted to sustain the high superficial thermal loads, are high velocity water cooled tubes, equipped with swirl tapes to increase their heat transfer capabilities. Figure 1 shows the model of the entire divertor assembly.

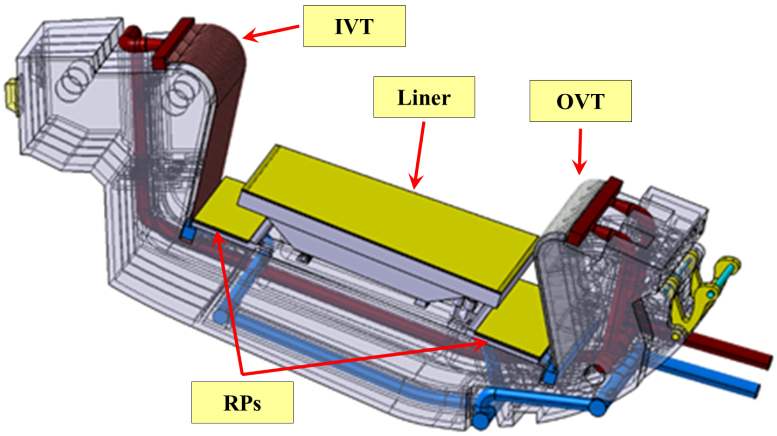

Figure 1. The DEMO divertor assembly.

Given this background, in the frame of the activities of the DEMO work package DIV-1 "Divertor Cassette Design and Integration", of the EUROfusion program aimed at developing a holistic divertor design concept [5], a mock-up of the OVT [6] of the DEMO divertor was built by the ENEA research group, mainly in order to:

- Demonstrate the technical feasibility of manufacturing procedures, focusing the attention on the joining/welding techniques, and optimizing costs of each component applying standard practices;
- Experimentally characterize the hydraulic behavior of the plasma facing components;
- Validate the computational fluid-dynamic (CFD) model developed at the University of Palermo against experimental data.

In this context, a research campaign was jointly carried out by the University of Palermo and ENEA to experimentally and theoretically assess the hydraulic performances of the OVT mock-up, paying particular attention to the coolant distribution among the PFUs and the total pressure drop across the inlet and outlet sections of the mock-up. Both the experimental and the theoretical–numerical campaigns will be extensively described in the following.

In particular, Section 2 is devoted to the description of the experimental test campaign carried out at ENEA Brasimone Labs, providing a brief overview of the CEF1 (Circuito per Esperienze di Fluidodinamica 1) water facility as well as of the OVT full-scale prototype and instrumentation. The attention is then focused on the obtained results, mainly in terms of pressure drops and mass flow rate distribution in the plasma facing cooling tube array.

On the other hand, Section 3 reports the comprehensive validation activity of the 3D CFD calculations carried out at the University of Palermo, based on the data obtained by the ENEA Brasimone Team from the experimental campaign on the OVT mock-up cooling circuit. The computational campaign was performed following a theoretical–numerical approach based on the finite volume method and adopting the well-known ANSYS CFX 2020 R2 commercial CFD code [7].

2. Experimental Test Campaign

In 2020, after the partial upgrade of the experimental hall at ENEA Brasimone laboratories, the complete design and realization of a new test section data and acquisition system and the installation of the OVT mock-up, the experimental test campaign was started by means of the CEF1 water loop, according to the test matrix drafted in [6]. The CEF1 water loop consists of a heat exchanger and two centrifugal pumps, which can be operated in series or in parallel, the test section, and the return line to the pressurized tank [6], as shown in Figure 2.

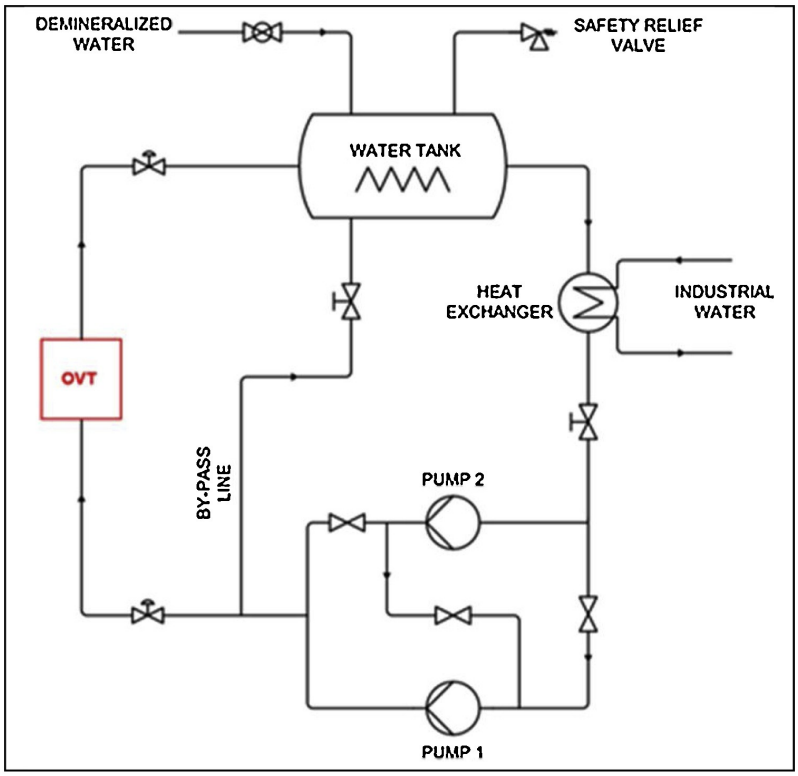

Figure 2. Simplified scheme of the CEF1 facility.

The OVT mock-up main components are the plasma facing channels, consisting of 39 tubes in CuCrZr equipped with internal helical swirl tape made of copper, the inlet/outlet manifolds made of AISI-316L steel, the inlet diffuser made of AISI-316L, the outlet header made of AISI-316L, the transition CuCrZr/AISI-316L tubes, i.e., the connection between the CuCrZr plasma facing tubes and AISI-316L manifolds/diffuser, and the supporting system [6]. Figure 3 shows the CAD model of OVT mock-up and its main components.

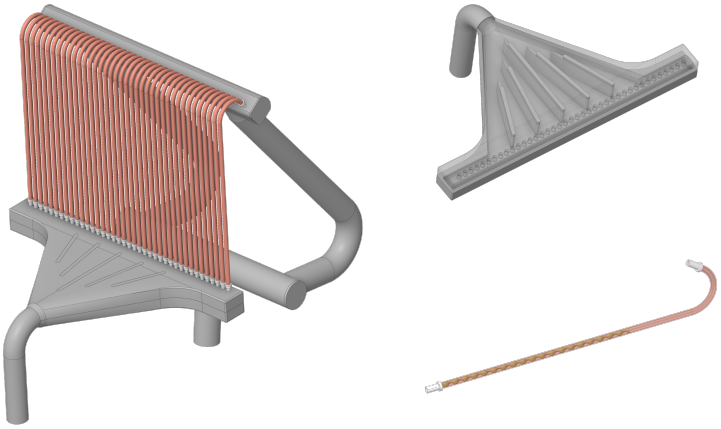

Figure 3. CAD model of the OVT mock-up (**left**), diffuser (**top right**), PFU channel (**bottom right**).

Even if small differences are present in the diffuser and the horizontal headers, mainly due to manufacturing constraints, the OVT cooling circuit exhibits the same structure as the corresponding DEMO divertor OVT [6]. Logically, the tungsten tiles and the copper interlayer were not considered because they were irrelevant for the planned test campaign [6].

Furthermore, certified and calibrated instrumentation was installed in the mock-up and used during the tests. It was mainly composed of two K-type thermocouples, measuring water temperatures at the inlet and outlet manifolds with a precision of ± 1 °C, a differential pressure transmitter measuring the mock-up total pressure drop with a precision of ± 0.001 bar, and a pressure transmitter at the inlet section with a precision of ± 0.012 bar. The positions of the thermocouples and of the differential pressure transmitter are shown in Figure 4.

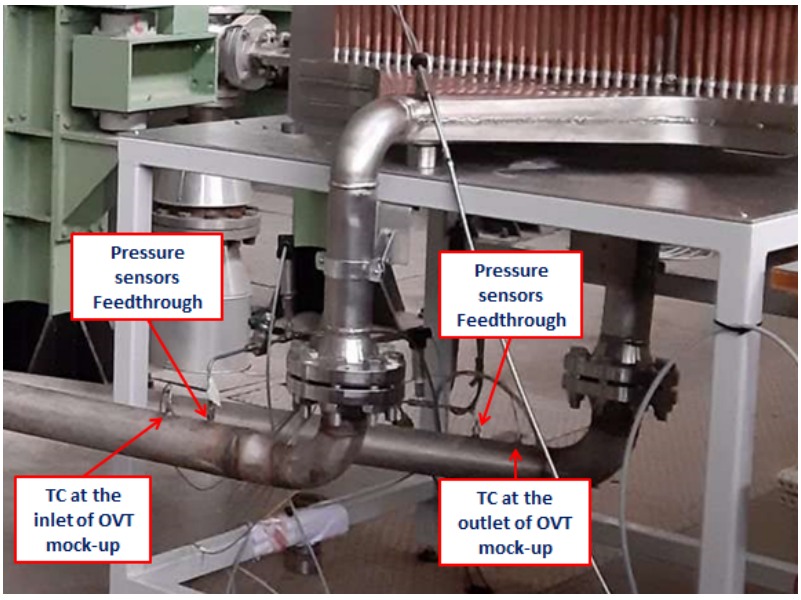

Figure 4. Detail of the thermocouples and of the differential pressure transmitter.

In addition, a new ultrasonic flow meter FLEXIM F601 [8] was acquired to measure coolant mass flow rates inside each of the 39 plasma facing tubes and it was placed downstream of the swirl tape location [6]. Figure 5 shows two pictures of the ultrasonic flow meter sensor installation on the upper part of the tube where the water flow is not disturbed, because it is far enough from the swirl tape, and the measurements are stable and reliable.

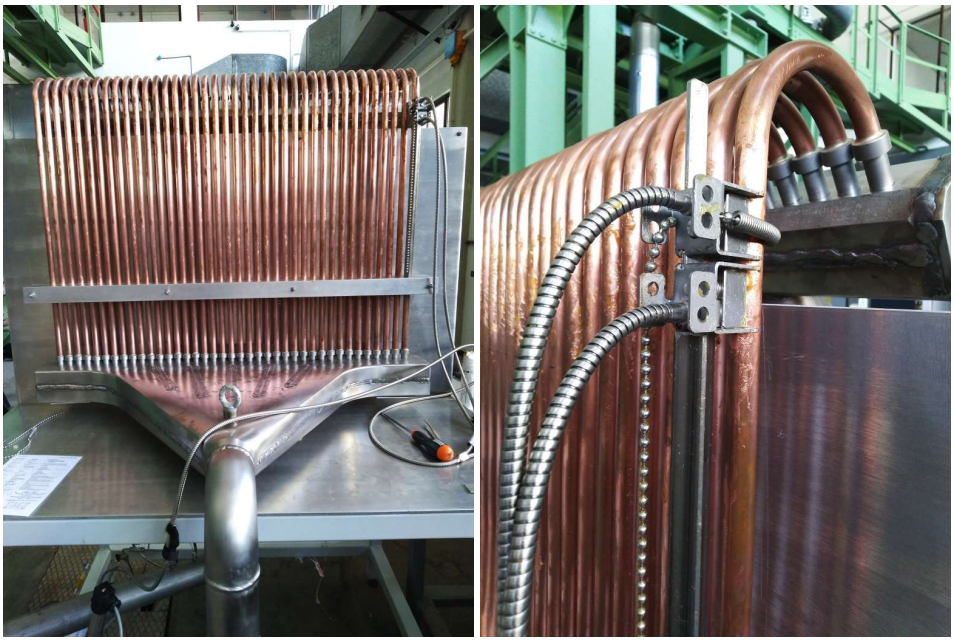

Figure 5. Ultrasonic flow meter measurements on the first OVT plasma facing cooling tubes.

The prototype mechanically connected to the water loop, instrumented, and ready for the test campaign is shown in Figure 6.

Figure 6. DEMO divertor OVT prototype installed into the CEF1 building.

Steady-State Tests

As for previous test campaigns performed on the ITER divertor cassette full-scale prototype [9], steady-state tests were carried out in order to determine the hydraulic characteristic function of the OVT mock-up cooling circuit, representing the functional dependence of the total pressure drop along the component, Δp_{tot}, on the corresponding mass flow rate, G, and at a given coolant temperature, T. In particular, tests at four different temperatures (20, 40, 70, and 100 °C) were performed, and for each temperature, five mass flow rate points were acquired from ≈15 kg/s to ≈35 kg/s, while inlet pressure ranged from ≈2 bar to ≈13 bar.

Table 1 summarizes the mock-up total pressure drops measured at different temperatures and mass flow rates. The pressure drop values were averaged over 240 s of data acquisition, in which the mass flow rate, as well as the temperature of the water loop, were kept constant, in order to make sure that quasi steady-state conditions were reached inside the experimental test section. Quasi steady-state conditions were typically reached in a few minutes.

Table 1. Summary of experimental steady-state results.

T [°C]	G [kg/s]	Δp_{Exp} [bar]
20	12.438 ± 0.191	0.510 ± 0.015
	20.223 ± 0.202	1.268 ± 0.013
	25.169 ± 0.188	1.845 ± 0.013
	30.087 ± 0.152	2.567 ± 0.041
	35.041 ± 0.186	3.393 ± 0.058
40	14.513 ± 0.073	0.650 ± 0.006
	22.560 ± 0.113	1.514 ± 0.059
	25.035 ± 0.125	1.821 ± 0.022
	30.135 ± 0.151	2.535 ± 0.040
	34.912 ± 0.175	3.325 ± 0.061
70	15.146 ± 0.076	0.665 ± 0.007
	20.346 ± 0.102	1.162 ± 0.014
	25.521 ± 0.134	1.770 ± 0.026
	30.282 ± 0.152	2.419 ± 0.044
	34.984 ± 0.175	3.212 ± 0.064
100	13.087 ± 0.066	0.498 ± 0.007
	19.705 ± 0.099	1.061 ± 0.023
	25.505 ± 0.128	1.723 ± 0.027
	30.221 ± 0.151	2.384 ± 0.049
	34.974 ± 0.182	3.126 ± 0.062

Afterwards, at each considered temperature, the hydraulic characteristic functions were derived by best fitting these results with the following analytical form:

$$\Delta p_{tot}(G) = \alpha G^{\beta} \quad (1)$$

where α and β are coefficients whose best-fitting values α_{Exp} and β_{Exp}, in SI units, are listed in Table 2.

The overall OVT prototype pressure drop obtained by extrapolating at the reference mass flow rate of 54.95 kg/s, Δp_{Exp}, is reported in Table 2 for each coolant temperature investigated. As it can be observed, they are close to their expected design value of 7.403 bar.

Table 2. OVT extrapolated pressure drops for the different test temperatures at the reference mass flow rate of 54.95 kg/s.

T [°C]	α_{Exp} [bar/(kg/s)$^{\beta}$]	β_{Exp} [-]	Δp_{Exp} [bar]
20	5.20×10^{-3}	1.8253	7.798
40	4.60×10^{-3}	1.8520	7.864
70	4.10×10^{-3}	1.8728	7.437
100	4.00×10^{-3}	1.8720	7.232

In parallel, the flow distributions among the plasma facing channels were experimentally determined by using the ultrasonic flow-meter FLEXIM F601. This detector uses an acoustic signal with ultrasonic frequency, which is sent and received through the liquid and measured by a pair of sensors properly placed on the pipe. The time needed for the acoustic signal to cross the liquid back and forth is directly proportional to the speed of the liquid and, hence, to its flow rate. The coolant mass flow rate was measured within each plasma facing tube only once quasi steady-state conditions were reached.

As shown in Figure 7, the mass flow rate distribution among the plasma facing channels is quite uniform and within the ±10% of its average value, corresponding to

maximum axial velocity values in the order of ≈9 m/s at the highest considered mass flow rate.

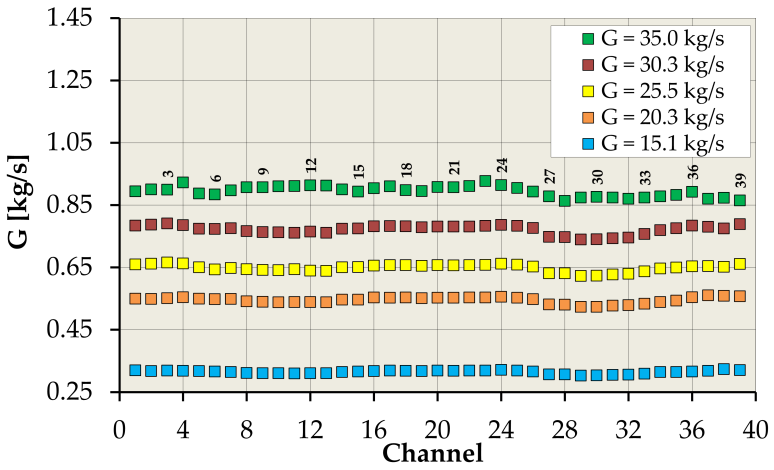

Figure 7. Ultrasonic flow meter measurements on 39 OVT plasma facing tubes at 70 °C (raw data, passed to the numerical simulation team).

3. OVT Mock-Up Cooling Circuit CFD Analysis

One of the main purposes behind the fabrication of the OVT mock-up was the experimental validation of the CFD models developed at the University of Palermo, in order to verify the computationally predicted hydraulic performances. Within this framework, a comprehensive validation activity of the 3D CFD calculations was carried out at the University of Palermo, based on the data obtained at the ENEA Brasimone Labs from the experimental campaign on the OVT mock-up cooling circuit. The computational campaign was performed following a theoretical–numerical approach based on the finite volume method and adopting the well-known ANSYS CFX 2020 R2 commercial CFD code [7].

In particular, in the first phase, a grid independence study was carried out, in order to quantify the discretization errors and to ensure numerical predictions in the asymptotic range of convergence.

Then, computational results were compared to the experimental outcomes, specifically in terms of coolant water velocity distribution in the entire PFU cooling tube array and total pressure drop of the mock-up cooling circuits.

Furthermore, a parametric analysis campaign was performed to evaluate how the uncertainties on the equivalent sand grain wall roughness may affect both total pressure drop and mass flow rate distribution among PFU channels.

It is worth mentioning how the mesh independence study and the uncertainty assessment on the equivalent sand grain wall roughness were performed to provide a measure of the degree of confidence on the outcomes of the numerical campaign.

Results obtained are herewith reported and critically discussed, together with the main assumptions, models, and boundary conditions (BCs).

3.1. Model Setup

To perform a validation campaign on the methodologies adopted for CFD simulation, steady-state isothermal CFD analyses were carried out on the OVT mock-up cooling circuit, whose geometry is reported in Figure 8, considering the assumptions and BCs reported in Tables 3 and 4.

With regard to Table 3, it is worth highlighting that the k-ω based SST model was adopted because it gives an accurate description of the near-wall region [7], especially in the case of flow separation. It is a hybrid model that uses a transformation of the k–ϵ model into a k–ω model in the near-wall region and the standard k–ϵ model in the fully turbulent region far from the wall. Moreover, this model uses the automatic wall treatment that

automatically switches from wall-functions to a low-Re near-wall formulation as the mesh is refined. The accuracy and the flexibility of the k-ω based SST model makes it suited for the analysis of very complex domains where a wide range of Reynolds numbers may be encountered and flow separation may occur. For further information, the interested reader is addressed to the code documentation [7].

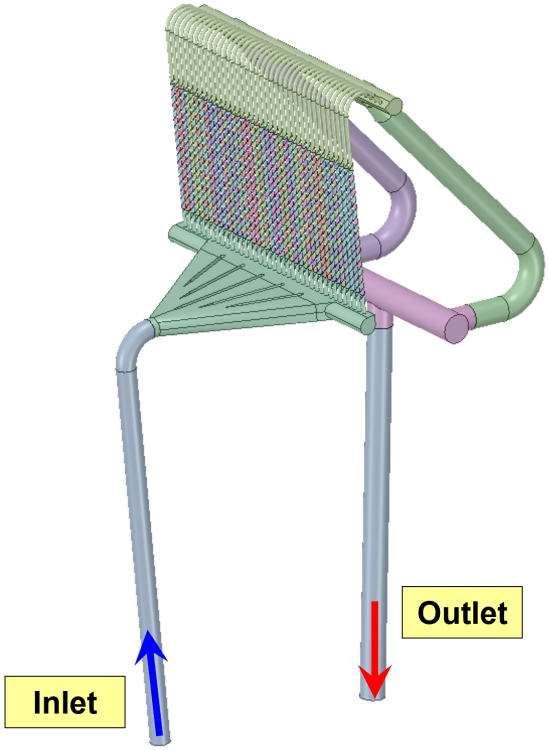

Figure 8. OVT mock-up cooling circuit calculation domain.

Among the wide range of operative conditions tested on the OVT mock-up cooling circuit at ENEA Brasimone Labs, attention was placed on the experimental tests performed at ≈20 °C inlet temperature (see Table 4). Under the selected operating conditions, the flow field inside the PFU channels was characterized by values of the Reynolds Re numbers (calculated according to the definition given in [10]), ranging between 3×10^4 and 1×10^5, resulting in a fully turbulent flow. Similar results in terms of Re were obtained for the manifold pipes.

Table 3. Summary of OVT mock-up CFD analysis setup.

	Reference Conditions
Analysis type	Steady-state isothermal
Material library	Water IAPWS IF97 [11]
Turbulence model	k-ω SST [7]
Differencing scheme	High-resolution [7]
Boundary layer modeling	Automatic wall functions [7]
PFU channels absolute wall roughness	2 µm
ST absolute wall roughness	2 µm
Other regions absolute wall roughness	15 µm
Inlet BC (temperature/pressure)	Variable according to Table 4
Outlet BC (mass flow rate)	

Table 4. List of selected experimental tests.

Test # [-]	p_{in} [bar]	G [kg/s]	T_{in} [°C]
1	1.42	12.27	17.85
2	3.92	21.27	20.38
3	5.93	25.29	21.61
4	8.73	30.09	24.06
5	12.09	35.05	25.33

3.2. Mesh Independence Studies

To evaluate and minimize the discretization error related to the CFD simulations, a grid independence study was preliminarily performed and the mesh-related error was assessed by adopting the well-established grid convergence index (GCI), both according to its original derivation, presented in [12], and considering the least-squares (LS) error estimation described in [13].

Four different increasingly refined meshes were considered, whose details are summarized in Table 5. These meshes were created with mixed tetrahedral and prism elements (see Figure 9), maintaining unchanged both the total number of layers and the first layer thickness, and adapting the layer growth rate to have a smooth transition between the bulk mesh and the last prism layer. Despite the limitations imposed by the adoption of tetra elements, the meshes were created with the aim of obtaining computational grids as similar as possible, in compliance with the requirements of ANSYS CFX, in terms of element quality. With regard to Table 5, it is worth highlighting how the average mesh quality metrics are within the acceptable ranges prescribed in [7], and less than 1% of the overall number of cells is characterized by poor metrics. As a consequence, mesh quality is not expected to significantly influence the results.

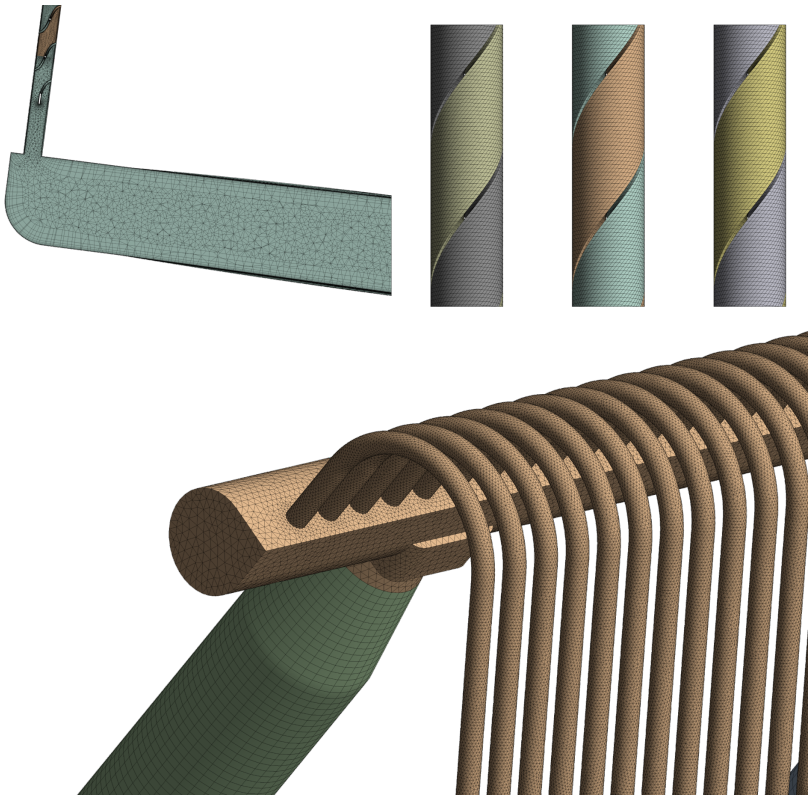

Figure 9. Finest mesh adopted for OVT mock-up cooling circuit CFD analyses.

Table 5. Adopted mesh parameters and quality metrics.

	Mesh #1	Mesh #2	Mesh #3	Mesh #4
Element size OVT/PFUs [mm]	10.4/1.3	8.0/1.0	6.15/0.77	4.73/0.59
First layer thickness [μm]	20			
Surface with y^+<10 at Test #5 [%]	≈80			
Number of layers [-]	12			
Layer growth rate OVT/PFUs [-]	1.68/1.42	1.65/1.39	1.61/1.36	1.58/1.33
Number of nodes [-]	1.42×10^7	2.09×10^7	3.22×10^7	4.15×10^7
Number of elements [-]	2.05×10^7	2.78×10^7	4.03×10^7	5.14×10^7
Node density [m^{-3}]	3.25×10^8	4.81×10^8	7.40×10^8	9.53×10^8
Orthogonality Factor (average/min)	0.59/0.01	0.61/0.01	0.67/0.01	0.72/0.01
Expansion factor (average/max)	2/617	2/607	2/299	2/258
Aspect ratio (average/max)	38/1830	29/1415	19/1582	17/1077

Additionally, the first layer thickness was selected sufficiently small to have the highest y^+ values in the order of the unity, to capture the entire boundary layer profile. Some details of the resulting finest mesh (Mesh #4) are depicted in Figure 9.

All analyses were run until all residuals reached the iteration convergence control criterion of 10^{-4} and a second-order accurate numerical scheme was adopted, as suggested by [14].

On the other hand, the figure of merit (FoM) monitored and collected to assess the grid convergence is the total pressure drop between inlet and outlet sections of the OVT mock-up cooling circuit. The obtained results are summarized in Table 6.

Table 6. Outlook of the results obtained with the different meshes.

G [kg/s]	Δp_{Num} [bar]			
	Mesh #1	Mesh #2	Mesh #3	Mesh #4
12.27	0.500	0.475	0.462	0.460
21.27	1.394	1.335	1.303	1.296
25.29	1.935	1.851	1.816	1.812
30.09	2.687	2.575	2.509	2.509
35.05	3.597	3.454	3.367	3.358

Starting from the results reported in Table 6, the GCI together with the asymptotic values obtained with the generalized Richardson extrapolation (that will be referred to simply as asymptotic values in the following) were calculated by adopting the procedure described in [12]. In particular, given a general monitored quantity ϕ, it can be related to the average mesh size by the following equation:

$$\phi_i = \phi_0 + \alpha h_i^{\rho}, \tag{2}$$

where ϕ_i is the measured value obtained with a selected mesh of average linear size h_i, ϕ_0 is the estimate of the asymptotic value, α is a constant and ρ is the observed order of convergence. Given the results obtained with a set of three meshes, it is then possible to obtain, by proper interpolation, the values of ϕ_0, α and ρ.

The GCI can therefore be calculated for the selected i-th grid, as follows

$$GCI_i = F_s \left| \frac{\phi_i - \phi_0}{\phi_i} \right| = F_s \left| \frac{\alpha}{\phi_i} \right| h_i^{\rho}, \tag{3}$$

where F_s can be interpreted as a safety factor, conservatively chosen here equal to 3.

It is important to remark that the observed order of convergence should be within the acceptable range for a second-order accurate numerical method. A value greater than

this formal order of convergence is likely to cause too small error estimates [13], as can be easily deduced from Equation (3), being $h_i \ll 1$.

The outcomes of the analyses showed good monotonically convergent behavior, with the highest GCI calculated according to [12] being ≈1.5%, suggesting results close to their asymptotic values. Moreover, an observed order of convergence ρ within the range 8–50 was calculated, clearly outside the above-mentioned suitable limits, and possibly related to noisy results. The procedure described in [13] was therefore considered, with the aim to estimate more conservative and realistic GCI values by obtaining a better estimate of ρ. This can be accomplished since this method evaluates the parameters ϕ_0, α and ρ of Equation (2) in an LS sense, performing a best-fitting of the results obtained; thus, limiting the effects of scattered data. In case unduly high or low ρ-values are calculated, this method prescribes that a best-fitting with both linear and quadratic functions is performed. The results obtained by adopting this approach are summarized as follows:

- The observed convergence order ranges between 7.80 and 10.43, lower than the results obtained with the classical GCI formulation, yet outside the prescribed limits;
- GCI values calculated adopting the parameters obtained with the LS approach result between 1 and 2.7% for all of the considered mass flow rates, and are characterized by a lower spread compared to the outcomes of the original GCI formulation;
- The prescribed best-fittings with linear and quadratic functions resulted in unrealistic and underestimated asymptotic values, not compatible with the experimental results and, consequently, in excessively high GCI values.

Therefore, the outcomes of these latter fittings were discarded, and it can be reasonably argued from the results obtained shown that an observed order of convergence of ≈8 realistically characterizes the examined problem. To further confirm this assumption, an additional fine mesh of approximately 10^8 elements was tested and, due to the huge computational time required, only one simulation, the one with the lowest mass flow rate, was considered. The results obtained (see Figure 10) prove that the calculated observed order of convergence can be reliably adopted to realistically estimate the GCI, resulting in the additional tested mesh well-predicted by the LS fitting.

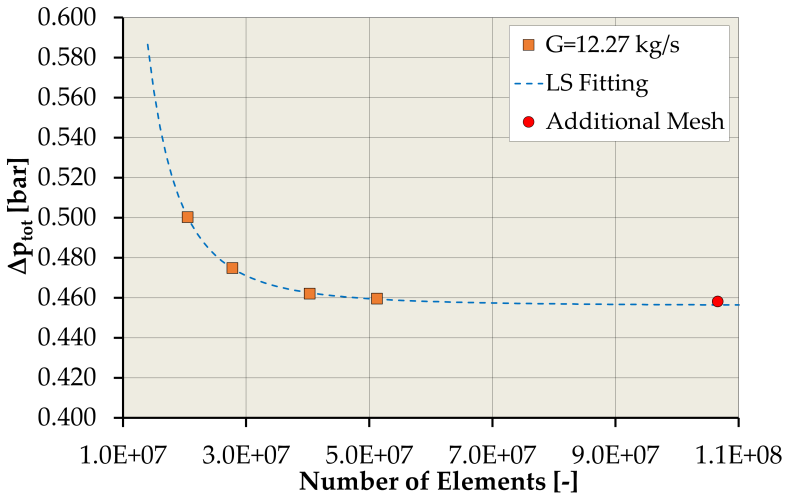

Figure 10. Grid independence results obtained for a mass flow rate of 12.27 kg/s.

The outcomes of the entire mesh independence analysis are summarized in Table 7, while the relative errors with respect to the pertaining asymptotic values are reported in Figure 11. As a closing remark, it can be safely and conservatively stated that the results obtained with Mesh #4 are characterized by a small discretization error, which can be reasonably considered below 3%.

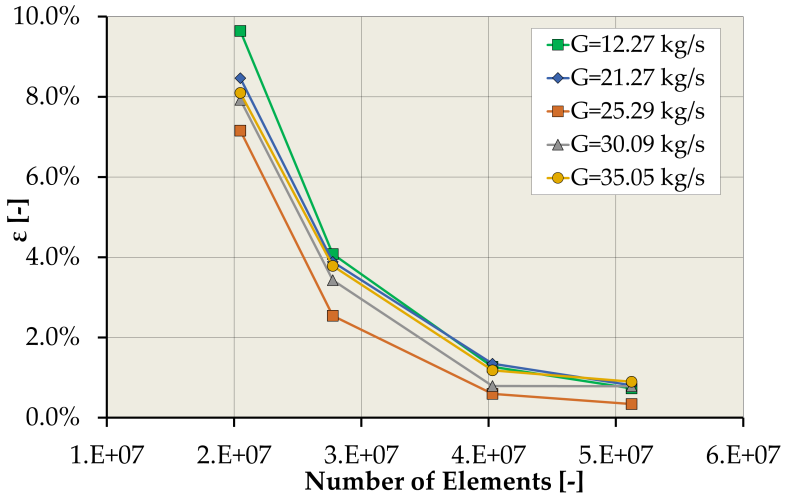

Figure 11. Relative error with respect to the LS asymptotic values.

Table 7. Overview of the grid independence studies.

G [kg/s]	Original GCI Formulation			LS GCI Formulation		
	Asymptotic Values	ρ	GCI [%]	Asymptotic Values	ρ	GCI [%]
12.27	0.458	9.43	1.31	0.456	8.53	2.18
21.27	1.289	8.54	1.52	1.285	7.80	2.40
25.29	1.809	12.31	0.42	1.805	10.43	1.01
30.09	2.509	49.77	0.00	2.489	8.73	2.34
35.05	3.353	13.81	0.38	3.328	7.81	2.67

3.3. Results and Comparison with Experimental Data

The results of the OVT mock-up cooling circuit CFD analysis, considering the previously selected Mesh #4, are herein reported mainly in terms of coolant total pressure drop and mass flow rate distribution among PFU channels, and compared with the experimental data discussed in Section 2.

The coolant total pressure spatial distribution within the OVT mock-up cooling circuit, the details of the coolant flow velocity field inside the manifolds, and the PFU channels assessed for the 35.05 kg/s case are shown in Figure 12.

The comparison between the numerical predictions and the outcomes of the experimental campaign in terms of OVT mock-up characteristic curves, i.e., Equation (1), is reported in Figure 13, with the addition of 10% error bars, so to give an immediate view of the error, and is summarized in Table 8. From the analysis of the results, it may be argued that the maximum error on pressure drop estimation occurs at the lowest investigated flow rate and is equal to −7.22%, showing an overall good agreement between CFD simulations and experimental data.

Table 8. Total pressure drop comparison and errors.

G [kg/s]	Δp_{Num} [bar]	Δp_{Exp} [bar]	ϵ [%]
12.27	0.460	0.495	−7.22%
21.27	1.296	1.354	−4.32%
25.29	1.812	1.859	−2.56%
30.09	2.509	2.567	−2.26%
35.05	3.358	3.384	−0.77%

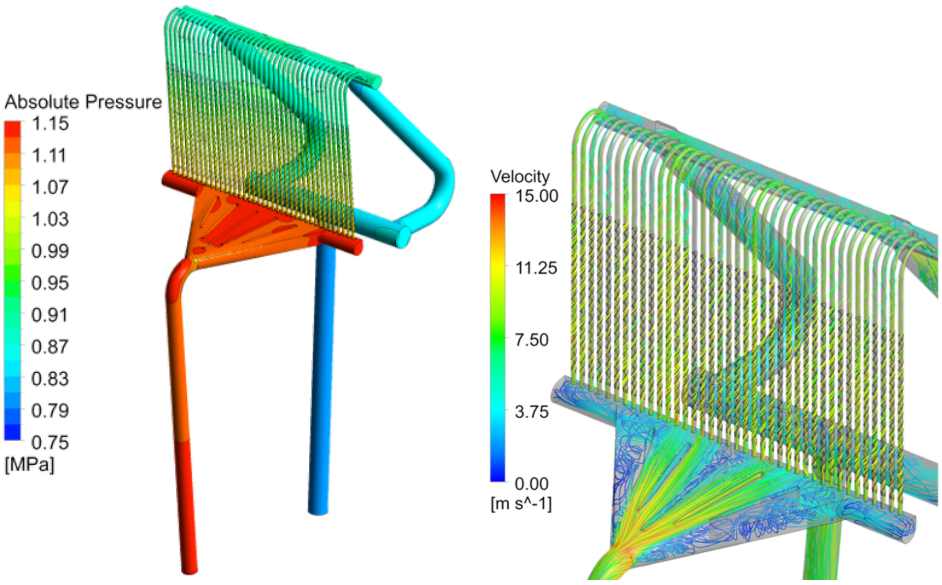

Figure 12. OVT mock-up results at G = 35.05 kg/s. OVT mock-up coolant total pressure field (**left**); OVT mock-up coolant flow velocity field (**right**).

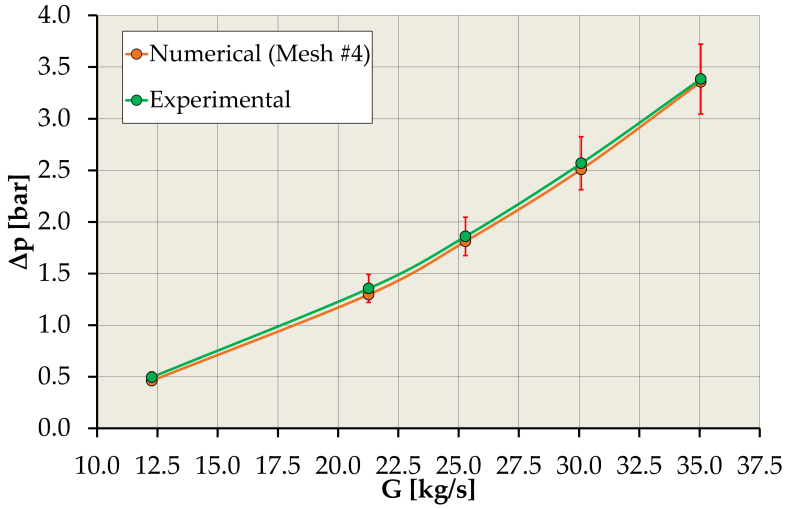

Figure 13. Numerical and experimental characteristic curves of the OVT mock-up cooling circuit.

The comparison between numerical and experimental mass flow rate distributions among the OVT mock-up PFU channels is reported for test #5 of Table 4 (being the one with the worst agreement between experimental and numerical outcomes) in Figure 14, with 5% error bars alongside the key parameters for all of the considered mass flow rates in Table 9 where, together with the maximum and minimum flow rates measured for the PFU channels, the standard deviations are reported σ, and the coefficient of variation, defined as:

$$C_{V,G} = \frac{\sigma}{G_{ave}}. \quad (4)$$

Additionally, maximum and average relative errors between experimental and numerical distributions among the OVT mock-up PFU channels are reported in Table 10.

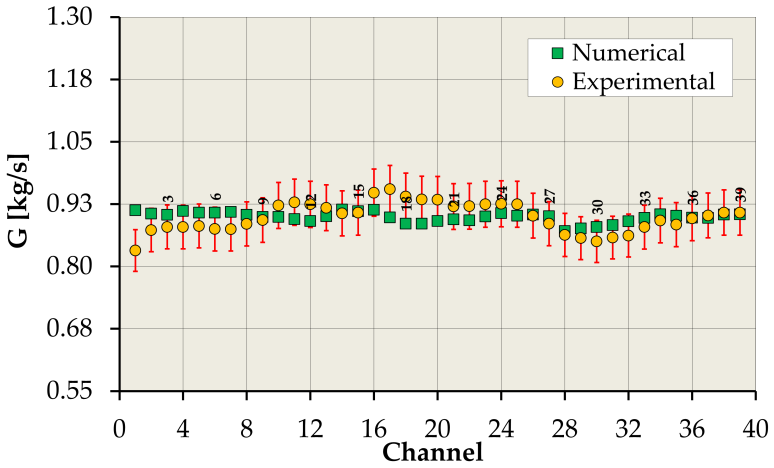

Figure 14. Comparison of OVT coolant mass flow rate distributions at G = 35.05 kg/s.

Table 9. Comparison of OVT coolant mass flow rate distribution main parameters.

		G_{Max}/G_{min} [kg/s]	σ [kg/s]	$C_{V,G}$ [%]
G = 12.27 kg/s	Numerical	0.323/0.303	0.005	1.59
	Experimental	0.331/0.229	0.008	2.54
G = 21.27 kg/s	Numerical	0.560/ 0.523	0.010	1.83
	Experimental	0.578/0.518	0.015	2.75
G = 25.29 kg/s	Numerical	0.666/0.622	0.012	1.85
	Experimental	0.686/0.617	0.014	2.16
G = 30.09 kg/s	Numerical	0.791/0.739	0.015	1.94
	Experimental	0.811/0.729	0.021	2.72
G = 35.05 kg/s	Numerical	0.921/0.863	0.016	1.78
	Experimental	0.955/0.832	0.029	3.23

Table 10. Maximum and average relative errors on mass flow rate distributions among OVT mock-up PFU channels.

G [kg/s]	ϵ_{Max} [%]	ϵ_{ave} [%]
12.27	5.90	2.29
21.27	8.22	2.23
25.29	4.35	1.40
30.09	7.63	3.11
35.05	9.36	2.20

From the analysis of the results, it might be argued that experimental data show a higher spread of flow distribution among PFU channels and a higher degree of asymmetry with respect to CFD results for all of the cases under investigation. Despite this discrepancy, the agreement between numerical and experimental results is quite good, and the maximum error is predicted for the 35.05 kg/s case simulation and is equal to 9.36% for PFU channel #1, while the average error has a maximum of 3.11% for the 30.09 kg/s case.

3.4. Sensitivity Analysis on the Equivalent Sand-Grain Wall Roughness

One of the major uncertainties in the accurate reproduction of experimental test conditions is the lack of precise knowledge on the equivalent sand grain wall roughness values of PFU channels, swirl tapes, and mock-up pipes and manifolds. Since equivalent sand grain wall roughness may have a strong impact on both total pressure drop and mass

flow distribution among the PFU channels, a parametric sensitivity analysis campaign was performed to evaluate how these uncertainties may affect the obtained results, by providing numerical estimates of the local sensitivity measures S:

$$S_{\Delta p_{tot},k_j} = \frac{1}{\Delta p_{tot,0}} \frac{\partial \Delta p_{tot}}{\partial k_j}\bigg|_{\underline{k_0}}, \quad S_{C_{V,G},k_j} = \frac{\partial C_{V,G}}{\partial k_j}\bigg|_{\underline{k_0}}, \tag{5}$$

where k_j are referred in turn to PFU channels, swirl tape, and mock-up pipes, and manifolds surface roughness values. The local derivatives of Equation (5) are taken at the baseline configuration, considering the surface roughness values of Table 3, referenced as $\underline{k_0}$ in Equation (5).

The baseline analyses were performed considering a surface roughness of 2 µm for both PFU channels and copper swirl tapes. This same value was already adopted for the thermal hydraulic assessment of the DEMO divertor PFC cooling circuit [15] and similar values can be found in literature [16,17]. The response of the OVT mock-up cooling circuit in terms of total pressure drop and mass flow rate distribution among PFU channels was therefore assessed, considering a small variation of this parameter around the baseline value. There were two different equivalent sand grain wall roughness values of 1 and 4 µm (halved and doubled with respect to baseline, respectively), separately for PFU channels and swirl tapes, with the aim to identify the component responsible for higher deviations of the results and to quantify their magnitude.

Regarding mock-up pipes and manifolds—the baseline surface roughness of 15 µm was selected in agreement with the values adopted for the DEMO divertor cassette body (see, for example, [18]). Since no better estimates of the roughness were available, it was deemed necessary to test the response of the CFD mock-up cooling circuit to a broader range of roughness values, and in particular, the two values 1.5 and 150 µm were selected. All calculations were performed considering Mesh #4 discussed in Section 3.2, and the wall treatment presented in [19], necessary when the surface roughness was large compared to the near-wall mesh, was adopted for the 150 µm simulation, thus avoiding grid variations that would have possibly required an additional mesh independence study.

A summary of the cases investigated, together with the baseline equivalent sand grain surface roughness vales, is given in Table 11.

Table 11. Absolute Hydraulic Wall Roughness values investigated.

	$\mathbf{k_{pipes}}$ [µm]	$\mathbf{k_{ST}}$ [µm]	$\mathbf{k_{manifolds}}$ [µm]
Baseline	2	2	15
PFU channels	1–4	2	15
Swirl tapes	2	1–4	15
OVT mock-up pipes and manifolds	2	2	1.5–150

The outcomes of the sensitivity analyses are summarized, for the sake of brevity, as follows.

- Due to the presence of non-stationary features of the fluid flow, such as the strongly detached flow inside the inlet manifold clearly visible in Figure 12 (right), an oscillation of the results is always observed in the simulations. As a consequence, the small variations in terms of total pressure drop and mass flow distribution among PFU channels observed by varying the surface roughness are hardly recognized from the noisy nature of the results. To obtain better estimates of the effects of surface roughness sensitivity, the outcomes reported in the following were calculated by averaging the metrics of Equation (5) obtained for the five different mass flow rate cases.
- Varying the PFU channels surface roughness, a variation of total pressure drop between −0.6% and +1.8% is detected. It results in an average of $S_{\Delta p_{tot},k_{pipes}} \approx 0.8\%/\mu m$.

- Varying the swirl tape surface roughness, a variation of total pressure drop between -0.4% and $+0.5\%$ is obtained. An average of $S_{\Delta p_{tot}, k_{ST}} \approx 0.3\%/\mu m$, lower than the sensitivity to PFU channels roughness.
- Varying the OVT mock-up pipes and manifolds surface roughness, an average $\approx -2.5\%$ total pressure drop change is observed with the 1.5 μm equivalent sand grain roughness. The 150 μm case predicted an average 0.4% reduction in total pressure drop with respect to baseline case. This latter result is mainly related to the different wall treatment adopted, whose effect should be further investigated. As a consequence, it is not possible to provide an estimate of the parameter $S_{\Delta p_{tot}, k_{manifolds}}$.
- No significant change in flow distribution, in terms of coefficient of variation, is observed modifying the surface roughness of PFU channels, swirl tape, and OVT mock-up pipes and manifolds, always resulting in a lower spread of the mass flow rates if compared to the experimental values. In particular, absolute variations within the range $\pm 0.1\%$ are predicted by the model, resulting in $S_{C_{V,G}, k_j} \approx 0.0\%/\mu m$.

In summary, the sensitivity analysis showed a limited dependency of the numerical results on the surface roughness of the various components within the explored range of values, with deviations mostly lower than 3% of the baseline results. Nonetheless, the OVT mock-up cooling circuit showed, in particular, a higher sensitivity to the PFU channel surface roughness that may be related to the higher flow velocities experienced by the fluid inside the channels, and to the centrifugal force caused by the swirl motion responsible for higher local velocities close to the pipe walls.

4. Conclusions

In the frame of the pre-conceptual design activities of the DEMO work package DIV-1 "Divertor Cassette Design and Integration" of the EUROfusion program, a research campaign was jointly carried out by the University of Palermo and ENEA to experimentally and theoretically assess the hydraulic performances of a mock-up of the divertor outer vertical target, paying particular attention to the coolant distribution among the PFUs and the total pressure drop across the inlet and outlet sections of the mock-up.

The paper presents the results of the steady-state hydraulic experimental test campaign performed at the ENEA Brasimone Research Center as well as the relevant numerical analyses performed at the Department of Engineering at the University of Palermo. The test facility, the experimental apparatus, the test matrix and the experimental results are widely described and critically discussed together with the theoretical model, its assumptions, and the analyses outcomes.

In particular, the experimental tests on the OVT prototype showed that the expected overall pressure drop at the reference mass flow rate of 54.95 kg/s is close to the previously calculated design value of 7.403 bar for each coolant temperature investigated. Furthermore, the mass flow rate distribution among the plasma facing channels is sufficiently uniform, being the maximum variation within the $\pm 10\%$ of the average value.

On the other hand, the theoretical–numerical analysis campaign started from a thorough mesh independence study that allowed selecting a mesh characterized by a small discretization error, i.e., below 3%. Afterwards, among the wide range of operative conditions tested on the OVT mock-up cooling circuit at ENEA Brasimone Labs, attention was placed on numerically reproducing the experimental tests performed at $\approx 20\ ^\circ C$ inlet temperature. The results exhibit an overall good agreement with experimental data, being the maximum error on pressure drop estimation equal to -7.22%. Similar conclusion may be drawn from the comparison of the coolant flow distributions among PFU channels since the maximum error is predicted to be 9.36%, while the average error has a maximum of 3.11%. In general, it may be argued that experimental data show a higher spread of flow distribution among PFU channels and a higher degree of asymmetry, with respect to CFD results for all of the cases under investigation. Furthermore, the final sensitivity analyses showed a limited dependency of the numerical results on the surface roughness of the

various components within the explored range of values, with deviations in the order of a few percent of the baseline results.

Author Contributions: Conceptualization, methodology, investigation, writing—original draft, A.T., F.M.C., M.C., P.A.D.M., I.D.P., D.M., G.M., A.Q., E.V., J.-H.Y. All authors have read and agreed to the published version of the manuscript.

Funding: This work was carried out within the framework of the EUROfusion Consortium and received funding from the Euratom Research and Training Programme 2014–2018 and 2019–2020, under grant agreement no. 633053. The views and opinions expressed herein do not necessarily reflect those of the European Commission.

Data Availability Statement: The data presented in this study are available on request from the corresponding author.

Conflicts of Interest: The authors declare no conflict of interest.

References

1. Donné, A.J.H.; Morris, W. *European Research Roadmap to the Realisation of Fusion Energy*; EUROfusion: Garching/Munich, Germany, 2018; ISBN 978-3-00-061152-0.
2. Donné, A.J.H. The European roadmap towards fusion electricity. *Philos. Trans. R. Soc.* **2019**, *377*, 20170432. [CrossRef]
3. Federici, G.; Bachmann, C.; Barucca, L.; Baylard, C.; Biel, W.; Boccaccini, L.V.; Bustreo, C.; Ciattaglia, S.; Cismondi, F.; Corato, V.; et al. Overview of the DEMO staged design approach in Europe. *Nucl. Fusion* **2019**, *59*, 066013. [CrossRef]
4. Mazzone, G.; You, J.H.; Bachmann, C.; Bonavolontà, U.; Cerri, V.; Coccorese, D.; Dongiovanni, D.; Flammini, D.; Frosi, P.; Forest, L.; et al. Eurofusion-DEMO Divertor—Cassette Design and Integration. *Fusion Eng. Des.* **2020**, *157*, 111656. [CrossRef]
5. You, J.H.; Mazzone, G.; Bachmann, C.; Coccorese, D.; Cocilovo, V.; De Meis, D.; Di Maio, P.A.; Dongiovanni, D.; Frosi, P.; Di Gironimo, G.; et al. Progress in the initial design activities for the European DEMO divertor: Subproject "Cassette". *Fusion Eng. Des.* **2017**, *124*, 364–370. [CrossRef]
6. Mazzone, G.; You, J.H.; Cerri, V.; Coccorese, D.; Garitta, S.; Di Gironimo, G.; Marzullo, D.; Di Maio, P.A.; Vallone, E.; Tincani, A.; et al. Structural verification and manufacturing procedures of the cooling system, for DEMO divertor target (OVT). *Fusion Eng. Des.* **2019**, *146*, 1610–1614. [CrossRef]
7. ANSYS Inc. *ANSYS CFX-Solver Theory Guide*; Release: 2020 R2; ANSYS Inc.: Canonsburg, PA, USA, 2020.
8. FLEXIM F601. Available online: https://www.flexim.com/en/product/fluxus-f601 (accessed on 1 December 2021).
9. Tincani, A.; Di Maio, P.A.; Dell'Orco, G.; Ricapito, I.; Riccardi, B.; Vella, G. Steady state and transient thermal hydraulic characterization of full-scale ITER divertor plasma facing components. *Fusion Eng. Des.* **2008**, *83*, 1034–1037. [CrossRef]
10. Manglik, R.M.; Bergles, A.E. *Swirl Flow Heat Transfer and Pressure Drop with Twisted-Tape Inserts*; Advances in Heat Transfer; Elsevier: Amsterdam, The Netherlands, 2003; Volume 36, pp. 183–266. [CrossRef]
11. International Association for the Properties of Water and Steam. *Revised Release on the IAPWS Industrial Formulation 1997 for the Thermodynamic Properties of Water and Steam*; IAPWS: Lucerne, Switzerland, 2007.
12. Roache, P.J. Verification of Codes and Calculations. *AIAA J.* **1998**, *36*, 696–702. [CrossRef]
13. Eça, L.; Hoekstra, M. A procedure for the estimation of the numerical uncertainty of CFD calculations based on grid refinement studies. *J. Comput. Phys.* **2014**, *262*, 104–130. [CrossRef]
14. Mahaffy, J.; Chung, B.; Song, C.; Dubois, F.; Graffard, E.; Ducros, F.; Heitsch, M.; Scheuerer, M.; Henriksson, M.; Komen, E.; et al. *Best Practice Guidelines for the Use of CFD in Nuclear Reactor Safety Applications*; NEA/CSNI/R(2014)11; International Atomic Energy Agency (IAEA): Vienna, Austria, 2015.
15. Di Maio, P.A.; Burlon, R.; Mazzone, G.; Quartararo, A.; Vallone, E.; You, J.H. Hydraulic assessment of an upgraded pipework arrangement for the DEMO divertor plasma facing components cooling circuit. *Fusion Eng. Des.* **2021**, *168*, 112368. [CrossRef]
16. Raffray, A.R.; Schlosser, J.; Akiba, M.; Araki, M.; Chiocchio, S.; Driemeyer, D.; Escourbiac, F.; Grigoriev, S.; Merola, M.; Tivey, R.; et al. Critical heat flux analysis and R&D for the design of the ITER divertor. *Fusion Eng. Des.* **1999**, *45*, 377–407. [CrossRef]
17. You, J.H.; Mazzone, G.; Visca, E.; Bachmann, C.; Autissier, E.; Barrett, T.; Cocilovo, V.; Crescenzi, F.; Domalapally, P.K.; Dongiovanni, D.; et al. Conceptual design studies for the European DEMO divertor: Rationale and first results. *Fusion Eng. Des.* **2016**, *109–111*, 1598–1603. [CrossRef]
18. Di Maio, P.A.; Garitta, S.; You, J.H.; Mazzone, G.; Vallone, E. Thermal-hydraulic study of the DEMO divertor cassette body cooling circuit equipped with a liner and two reflector plates. *Fusion Eng. Des.* **2021**, *167*, 112227. 112227. [CrossRef]
19. Aupoix, B. Roughness Corrections for the k–ω Shear Stress Transport Model: Status and Proposals. *J. Fluids Eng.* **2014**, *137*. [CrossRef]